星形成ゼミ #340 19-26

岩崎一成 (国立天文台)

19. **Gas infalling motions in the envelopes of Very Low Luminosity Objects**
20. **Efficiently Cooled Stellar Wind Bubbles in Turbulent Clouds I. Fractal Theory and Application to Star-Forming Clouds**
21. Efficiently Cooled Stellar Wind Bubbles in Turbulent Clouds II. Validation of Theory with Hydrodynamic Simulations
22. **A Low-mass Cold and Quiescent Core Population in a Massive Protocluster**
23. **A Multi-wavelength Study on the Formation of AFGL 333-Ridge**
24. Revealing Ionization Conditions of Sz 102 with Spatially Resolved [Ne III] Microjets
25. Do ultra compact dwarf galaxies form monolithically or as merged star cluster complexes?
26. PENELLOPE: the ESO data legacy program to complement the Hubble UV Legacy Library of Young Stars (ULLYSES) I. Survey presentation and accretion properties of Orion OB1 and σ-Orionis

19. **Gas infalling motions in the envelopes of Very Low Luminosity Objects**

Mi-Ryang Kim, Chang Won Lee, Maheswar, G, Philip C. Myers, Gwanjeong Kim

★ We present the results of a single dish survey toward 95 VeLLOs in optically thick (HCN 1-0) and thin (N_2H^+ 1-0) lines performed for the purpose of understanding the physical processes of inward motions in the envelopes of the VeLLOs and characterizing their true nature. The normalized velocity differences (δV_{HCN}) between the peak velocities of the two lines were derived for 41 VeLLOs detected in both lines. The δV distribution of these VeLLOs is found to be significantly skewed to the blue, indicating the dominance of infalling motions in their envelopes. The infall speeds were derived for 15 infall candidates by using the HILL5 radiative transfer model. The speeds were in the range of 0.03 km s^{-1} to 0.3 km s^{-1}, with a median value of 0.16 km s^{-1}, being consistent with the gravitational free-fall speeds from pressure-free envelopes. The mass infall rates calculated from the infall speeds are mostly of the order of $10^{-6} M_\odot\ yr^{-1}$ with a median value of $3.4 \pm 1.5 \times 10^{-6} M_\odot$ yr^{-1}. These are found to be also consistent with the values predicted with the inside-out collapse model and show a fairly good correlation with the internal luminosities of the VeLLOs. This again indicates that the infall motions observed toward the VeLLOs are likely to be due to the gravitational infall motions in their envelopes. Our study suggests that most of the VeLLOs are potentially faint protostars while two of the VeLLOs could possibly be proto-brown dwarf candidates.

次のページから紹介

背景

- **VeLLOs (Very Low Luminosity Objects)**
  - 以前はIRAS点源がないことから星なしコアだと思われていた天体の一部に、Spitzerによる高感度観測で極めて暗い中心天体が見つかった。Young+2004
  - 定義：原始星と似たSEDをしているが、暗い $L_{\rm int} < 0.2\,L_{\odot}$
  - 非常に若い原始星(まだ質量が小さく、降着が始まったばかり)？
    普通の原始星で、間欠的降着の静穏期にあたる？
    褐色矮星？
- この論文では、
  - VeLLOsのカタログ(Kim+2016)95天体のうち66天体を、
    HCN (1-0) 厚い輝線と N2H+ (1-0) 薄い輝線で観測して
    降着運動を統計的に調査 by KVN 21m radio telescope.
  - 42天体で両方の輝線を検出。残りの天体は一方だけ検出

- **輝線形状**
  - 光学的に薄い N2H+は単一ピークのガウシアン
  - 光学的に厚い HCNは、様々な形状を示す。
    - ダブルピークでblue asymmetry (48%)
    - ダブルピークでred asymmetry　(14%)
    - 広いwingがある。(27%)
    - 超微細構造輝線間の強度比がLTEで説明できない。

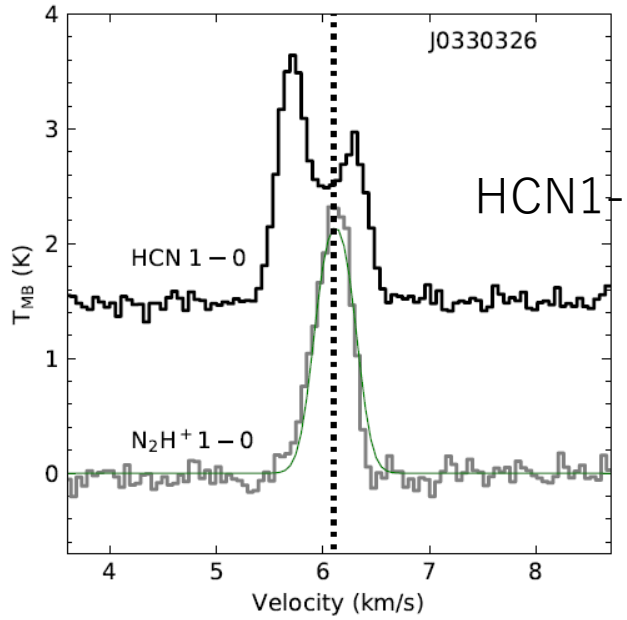

HCN1-0 (F=2-1)

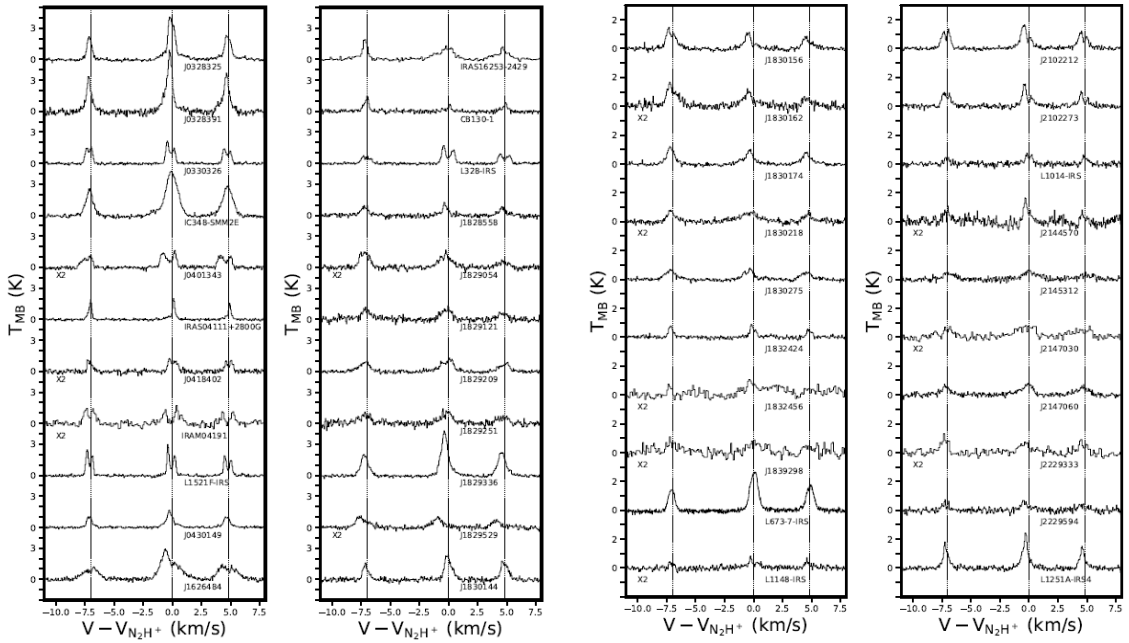

Infall motionで予言される輝線形状は、
blue asymmetry (Leung & Brown 1977, Myers 1996)

光学的に厚い場合は…

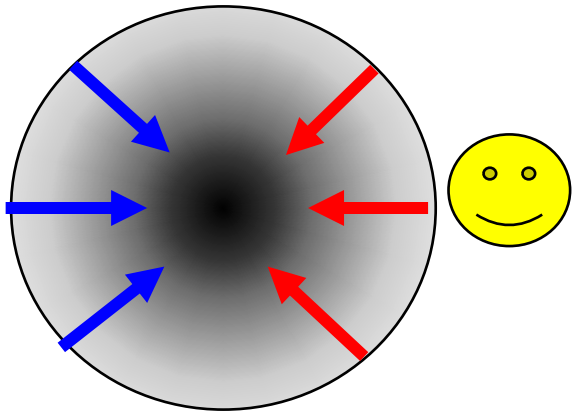

青方偏移した奥側：
- より密度が高い所が見える

赤方偏移した手前側
- より密度の低い所が見える

→ 青方偏移した方が強度が高く、
青方偏移側の方が、速度が系統的に
早い所を見ているので中心が
ちょっと青方にズレる

Infall運動 (輝線形状が綺麗な15天体)

- Vinfall-Vff関係
  - Vinfallは、輻射輸送モデル(HILL5, De Vries & Myers 2005)でfittingして導出。二つのガス層がVinfallで近づくモデル
  - Vffは密度が必要
    - コア質量(Hershel 250umから。TはHershelで求めた値。11.1-13.8K)

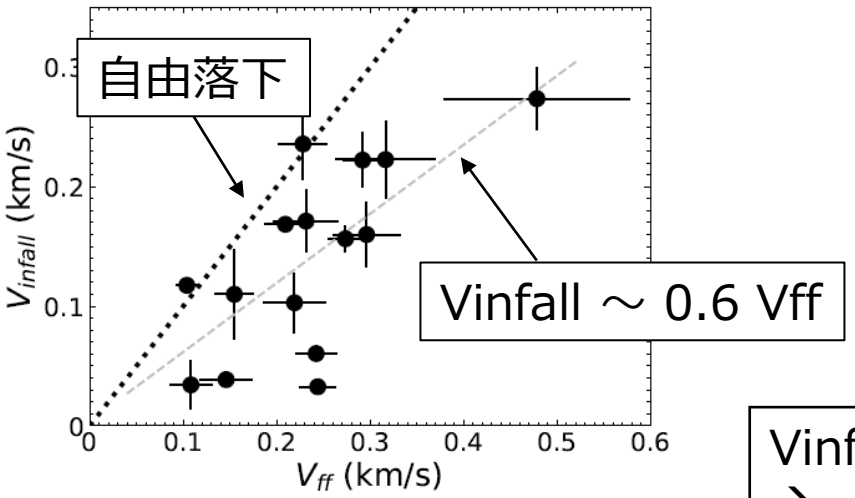

Figure 8. Comparison of the infall velocities for 15 cores with VeLLOs with their free-fall velocities. The black dotted line indicates the positions where V_{infall} is equal to V_{ff}. The grey dashed line is a line for the linear least-squares fit to the data. Its slope and Pearson correlation coefficient are 0.60±0.17 and 0.69, respectively.

VinfallとVffはよく相関
→
Vinfallは重力起源を示唆しているのではないか

$\dot{M}_{\rm acc}^{\rm CO} - \dot{M}_{\rm infall}$関係

- $\dot{M}_{\rm infall} = 4\pi R^2 \rho_0 V_{\rm infall}$で見積もる (外側)
- $\dot{M}_{\rm acc}^{\rm CO}$は、CO outflowから見積もる (内側)

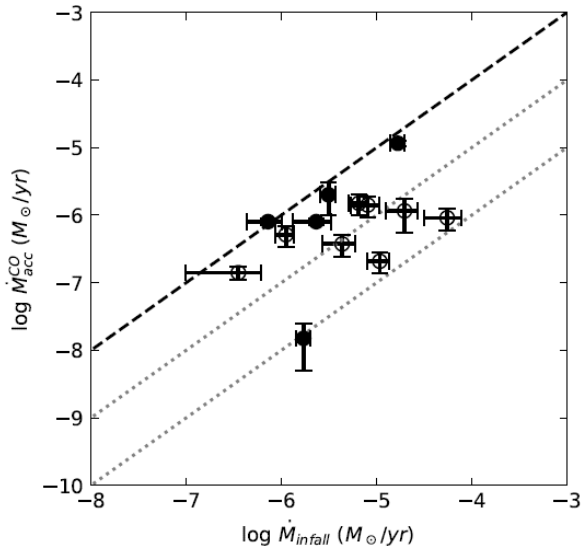

Figure 10. Mass infall rates versus the mass accretion rates toward the VeLLOs. The filled and open circles indicate the mass accretion rates obtained from CO observations in a mapping mode and a single pointing mode in CO line (Kim et al. 2019), respectively. The dashed and dotted lines are the positions where the ratios of $\dot{M}_{acc}^{CO}$ / $\dot{M}_{infall}$ are 1.0, 0.1 and 0.01, respectively.

- 半数くらい $\dot{M}_{\rm infall} \sim \dot{M}_{\rm acc}^{\rm CO}$
- 半数くらい $\dot{M}_{\rm infall} > M_{\rm acc}^{CO}$ → 静穏期？

Name	V_{infall}	V_{ff}	M_{env}	$M_{env}^{16''}$	$\dot{M}_{infall}$	$\dot{M}_{acc}^{CO}$	T_d	collapsing age	M_{acc}^{star}	M_{final}^{star}
	($km\ s^{-1}$)	($km\ s^{-1}$)	($M_\odot$)	($M_\odot$)	($M_\odot\ yr^{-1}$)	($M_\odot\ yr^{-1}$)	(K)	(Myr)	($M_\odot$)	($M_\odot$)
(1)	(2)	(3)	(4)	(5)	(6)	(7)	(8)	(9)	(10)	(11)
J032832	0.17±0.002	0.21±0.022	0.25±0.02	0.28±0.06	$6.5\pm1.4\times10^{-6}$	$1.5\pm5.0\times10^{-6*}$	12.5	0.11±0.01	0.17±0.06	0.22±0.06
J033032	0.06±0.004	0.24±0.022	0.65±0.05	0.38±0.06	$3.1\pm5.9\times10^{-6}$	$2.0\pm1.0\times10^{-6}$	11.5	0.12±0.01	0.24±0.12	0.37±0.13
J0418402	0.03±0.020	0.11±0.023	0.05±0.01	0.04±0.02	$3.5\pm2.5\times10^{-7}$	$1.4\pm3.0\times10^{-7*}$	12.5	0.06±0.01	0.008±0.002	0.02±0.01
L1521F-IRS	0.03±0.002	0.24±0.019	3.06±0.15	0.19±0.03	$1.7\pm2.9\times10^{-6}$	$1.5\pm1.0\times10^{-8}$	11.1	0.06±0.01	0.0009±0.0006	0.61±0.15
J0430149	0.12±0.002	0.10±0.012	0.03±0.01	0.03±0.01	$1.1\pm2.5\times10^{-6}$	$5.1\pm1.8\times10^{-7*}$	13.1	0.05±0.01	0.03±0.01	0.03±0.01
L328-IRS	0.04±0.005	0.15±0.028	0.07±0.02	0.10±0.04	$7.2\pm2.9\times10^{-7}$	$8.0\pm1.0\times10^{-7}$	13.1	0.08±0.01	0.07±0.01	0.08±0.02
J1830144	0.17±0.026	0.23±0.035	1.69±0.34	0.58±0.13	$8.1\pm2.7\times10^{-6}$	$1.4\pm5.0\times10^{-6*}$	12.6	0.19±0.04	0.27±0.11	0.61±0.35
J1830156	0.27±0.026	0.48±0.099	0.75±0.16	2.47±0.90	$5.5\pm2.3\times10^{-5}$	$9.1\pm3.2\times10^{-7*}$	12.9	0.19±0.04	0.17±0.07	0.66±0.90**
J1830162	0.22±0.033	0.32±0.053	0.43±0.09	1.08±0.29	$2.0\pm7.2\times10^{-5}$	$1.2\pm6.0\times10^{-6*}$	12.5	0.19±0.04	0.22±0.12	0.44±0.32**
J1832424	0.10±0.025	0.22±0.033	0.51±0.10	0.52±0.12	$4.3\pm1.7\times10^{-6}$	$3.7\pm1.3\times10^{-7*}$	13.8	0.18±0.04	0.07±0.03	0.17±0.11
L1148-IRS	0.11±0.038	0.15±0.021	0.32±0.02	0.19±0.05	$2.3\pm1.0\times10^{-6}$	$8.0\pm1.0\times10^{-7}$	12.3	0.14±0.01	0.11±0.02	0.18±0.02
J2102212	0.22±0.023	0.29±0.021	0.17±0.02	0.67±0.09	$1.7\pm2.9\times10^{-5}$	$1.2\pm1.0\times10^{-5}$	12.0	0.14±0.01	1.64±0.16	1.78±0.19**
J2102273	0.16±0.011	0.27±0.018	0.11±0.01	0.59±0.07	$1.0\pm1.5\times10^{-5}$	···	12.2	0.14±0.01	···	···
J2144570	0.16±0.027	0.30±0.036	1.96±0.11	1.53±0.37	$1.2\pm3.7\times10^{-5}$	···	12.5	0.31±0.01	···	···
J2229594	0.24±0.029	0.23±0.026	0.32±0.02	0.41±0.09	$1.1\pm2.8\times10^{-5}$	$2.1\pm7.0\times10^{-7*}$	12.1	0.14±0.01	0.03±0.01	0.11±0.09**

NOTE—Col.(1) lists the source name. Col.(2) gives the infall speed derived from HILL5 model fit for HCN (1-0) line. Its error is given by 1 σ uncertainty of the speed obtained from the HILL5 model fits for 1000 artificial spectra produced by the best fit parameters and observational rms. Col.(3) indicates free-fall speeds for the envelope by the area encompassed by the radius ($\sim 16''$) of the KVN telescope. Col.(4) gives the envelope mass which is based on the photometry with CSAR (Kim et al. 2016). Col.(5) lists the envelope mass based on the aperture photometry of 250 μm *Herschel* flux for the area encompassed by the radius ($\sim 16''$) of the KVN telescope. The uncertainty was calculated based on the photometry error. Col.(6) and Col.(7) provide the mass infall rate derived from the infall speed and the mass accretion rate inferred from CO outflow (Kim et al. 2019), respectively. The mass accretion rates marked with $*$ were derived from this study. Col.(8) lists the dust temperature and its $\sim 5\%$ uncertainty (Roy et al. 2014). Col.(9) indicates the period for the expansion sound wave in an isothermal sphere to travel to its radius which is half of our observing beam size in here(Shu 1977). Col.(10) lists the possible central mass of the VeLLOs to acquire with the mass accretion rates during the collapsing age given in Col.(9). Col.(11) indicates a possible final mass of the VeLLO to achieve, a sum of the possible central mass (in Col.(9)) plus the portion (~ 0.2) of the envelope mass (in Col.(4)). The stellar masses (M_{star}) with $**$ were calculated using the envelope mass given in Col.(5). The ellipsis symbols ($\cdots$) are to indicate "No outflow observation" and thus no further estimation of its corresponding physical quantities.

Shu解から

$$M_{\rm final} = \dot{M}_{\rm infall} \times t_{\rm collapse} + 0.2\ M_{\rm env}$$

褐色矮星候補天体

- VinfallとVff、($L_{\rm int} - \dot{M}_{\rm infall}$相関) → 重力収縮が有力
- $\dot{M}_{\rm infall} - \dot{M}_{\rm acc}^{\rm CO}$ 比較から、半数程度が静穏期にある？
- 二つの褐色矮星候補天体が見つかった。

20. **Efficiently Cooled Stellar Wind Bubbles in Turbulent Clouds I. Fractal Theory and Application to Star-Forming Clouds**

Lachlan Lancaster, Eve C. Ostriker, Jeong-Gyu Kim, Chang-Goo Kim

★ Winds from massive stars have velocities of 1000 km/s or more, and produce hot, high pressure gas when they shock. We develop a theory for the evolution of bubbles driven by the collective winds from star clusters early in their lifetimes, which involves interaction with the turbulent, dense interstellar medium of the surrounding natal molecular cloud. A key feature is the fractal nature of the hot bubble's surface. The large area of this interface with surrounding denser gas strongly enhances energy losses from the hot interior, enabled by turbulent mixing and subsequent cooling at temperatures $T = 10^4$-10^5 K where radiation is maximally efficient. Due to the extreme cooling, the bubble radius scales differently ($R \sim t^{1/2}$) from the classical Weaver (1977) solution, and has expansion velocity and momentum lower by factors of 10-10^2 at given R, with pressure lower by factors of 10^2 - 10^3. Our theory explains the weak X-ray emission and low shell expansion velocities of observed sources. We discuss further implications of our theory for observations of the hot bubbles and cooled expanding shells created by stellar winds, and for predictions of feedback-regulated star formation in a range of environments. In a companion paper, we validate our theory with a suite of hydrodynamic simulations.

- 星団による星風で駆動されるバブル進化を記述するモデル
- バブルのホットガスとシェルのあいだの乱流混合によって、冷却が効率的に効いて、古典的なWeaver+1977解からズレて、速度や運動量は10倍から100倍減少する。
- 理論の論文だったので紹介したかったけど、モデルが非常に込み入っていたので断念

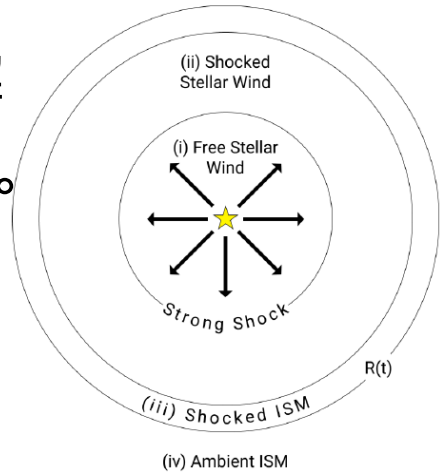

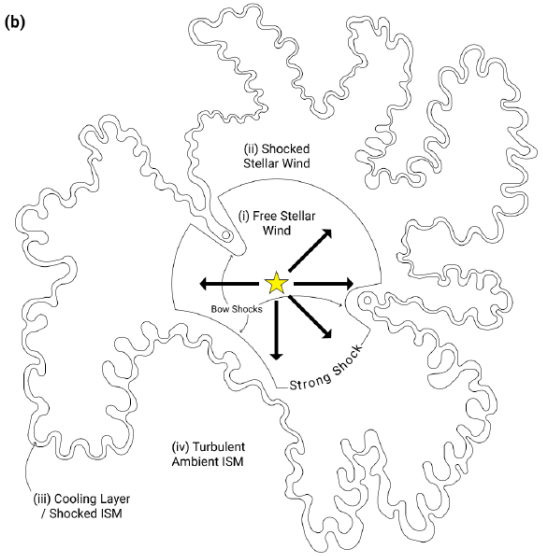

21. **Efficiently Cooled Stellar Wind Bubbles in Turbulent Clouds II. Validation of Theory with Hydrodynamic Simulations**

Lachlan Lancaster, Eve C. Ostriker, Jeong-Gyu Kim, Chang-Goo Kim ★
In a companion paper, we develop a theory for the evolution of stellar wind driven bubbles in dense, turbulent clouds. This theory proposes that turbulent mixing at a fractal bubble-shell interface leads to highly efficient cooling, in which the vast majority of the input wind energy is radiated away. This energy loss renders the majority of the bubble evolution momentum-driven rather than energy-driven, with expansion velocities and pressures orders of magnitude lower than in the classical Weaver (1977) solution. In this paper, we validate our theory with three-dimensional, hydrodynamic simulations. We show that extreme cooling is not only possible, but is generic to star formation in turbulent clouds over more than three orders of magnitude in density. We quantify the few free parameters in our theory, and show that the momentum exceeds the wind input rate by only a factor about 1.2-4. We verify that the bubble/cloud interface is a fractal with dimension about 2.5-2.7. The measured turbulent amplitude (v_t about 200-400 km/s) in the hot gas near the interface is shown to be consistent with theoretical requirements for turbulent diffusion to efficiently mix and radiate away most of the wind energy. The fraction of energy remaining after cooling is only $1\text{-}\Theta \sim 0.1\text{-}0.01$, decreasing with time, explaining observations that indicate low hot-gas content and weak dynamical effects of stellar winds.

- 20で作ったモデルの有効性を調べるとともに、パラメータを決める。
- 乱流混合によって冷却が加速され、注入された星風のエネルギーのうち0.1-0.01の割合しか残らず、運動量駆動段階が主に。

22 # A Low-mass Cold and Quiescent Core Population in a Massive Protocluster

Shanghuo Li, Xing Lu, Qizhou Zhang, Chang-Won Lee, Patricio Sanhueza, Henrik Beuther, Izaskun, Jiménez-Serra, Keping Qiu, Aina Palau, Siyi Feng, Thushara Pillai, Kee-Tae Kim, Hong-Li Liu, Josep Miquel. Girart, Tie Liu, Junzhi Wang, Ke Wang, Hauyu Baobab Liu, Howard A. Smith, Di Li, Jeong-Eun Lee, Fei Li, Juan Li, Shinyoung Kim, Nannan Yue, Shaye Strom

★ Pre-stellar cores represent the initial conditions of star formation. Although these initial conditions have been investigated in detail toward low-mass pre-stellar cores, such initial conditions remain vastly unexplored for massive star-forming regions. We report the detection of a cluster of low-mass starless and pre-stellar core candidates in a massive protocluster forming cloud, NGC6334S. With the ALMA observations at a ∼0.02 pc spatial resolution, we identified 17 low-mass starless core candidates that do not show any evidence of protostellar activity. These candidates present small velocity dispersions, high fractional abundances of NH_2D, high NH_3 deuterium fractionations, and are completely dark in the infrared wavelengths from 3.6 up to 70 μm. Turbulence is significantly dissipated and the gas kinematics are dominated by thermal motions toward these candidates. Nine out of the 17 cores are gravitationally bound, and therefore are identified as pre-stellar core candidates. The embedded cores of NGC6334S show a wide diversity in masses and evolutionary stages.

次のページから紹介

背景

- 重力的に束縛された星なしコアはpre-stellar coreと呼ばれ、星形成の始まりを表す天体だと考えられている。
- 小質量星形成領域のpre-stellar coreは近傍分子雲で詳細に調べられてきた。
- 一方で、大質量星団形成領域は、まだあま

→

本研究

- NGC6334S (IRDC G350.56+0.44)
  - 質量 1300 Msun (Li+2020)
- 観測
  - ALMA: $H^{13}CO^+$ (1-0), ortho $-NH_2D$ ($1_{11}-1_{0}$
    - NH2Dは、pre-stellar coreの高密度領域にも存在できるよいtracer
  - JVLA: $NH_3(1,0)$

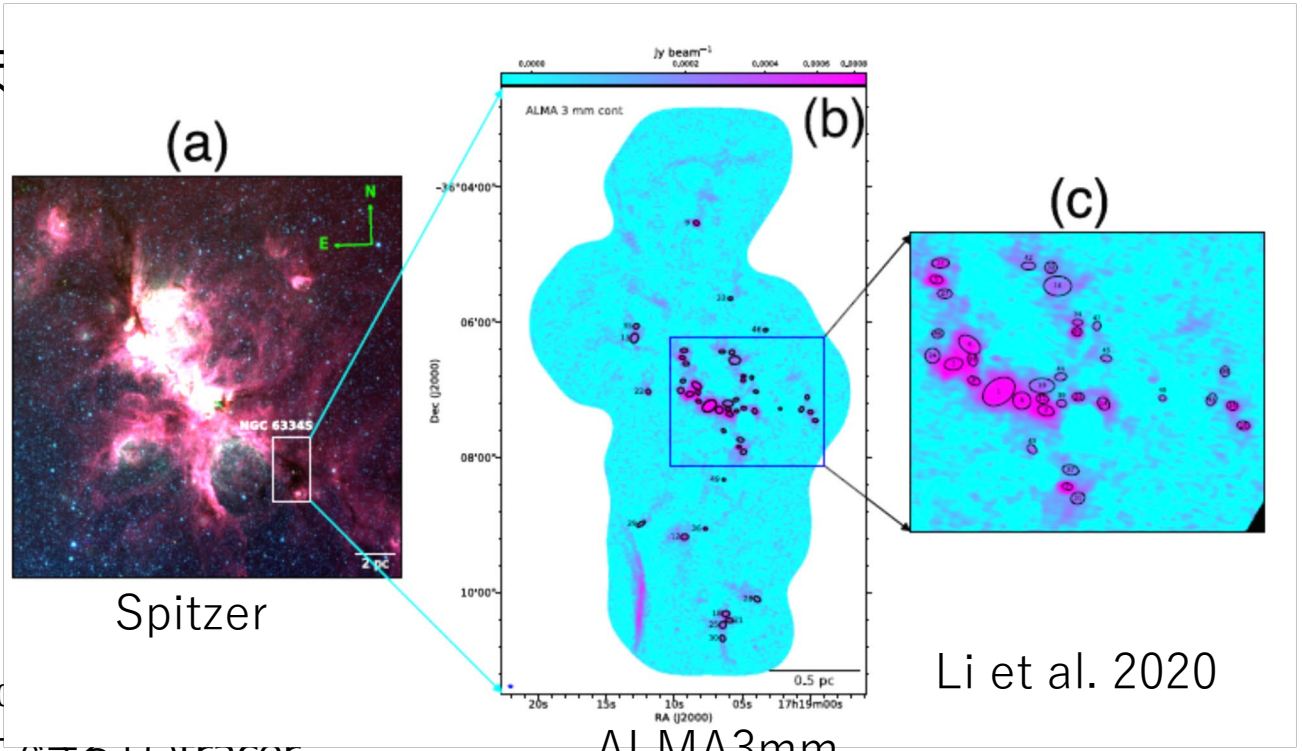

グレースケール：NH2Dの積分強度図

M1コア

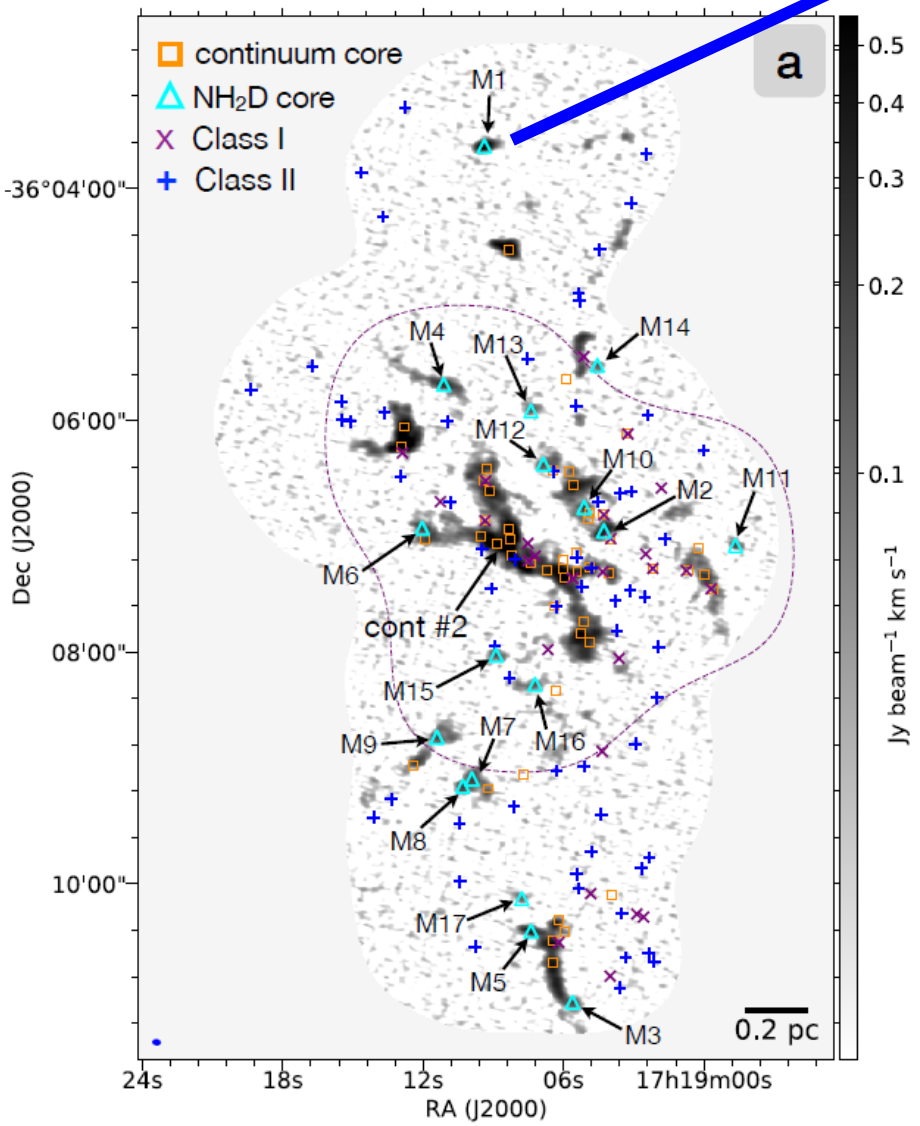

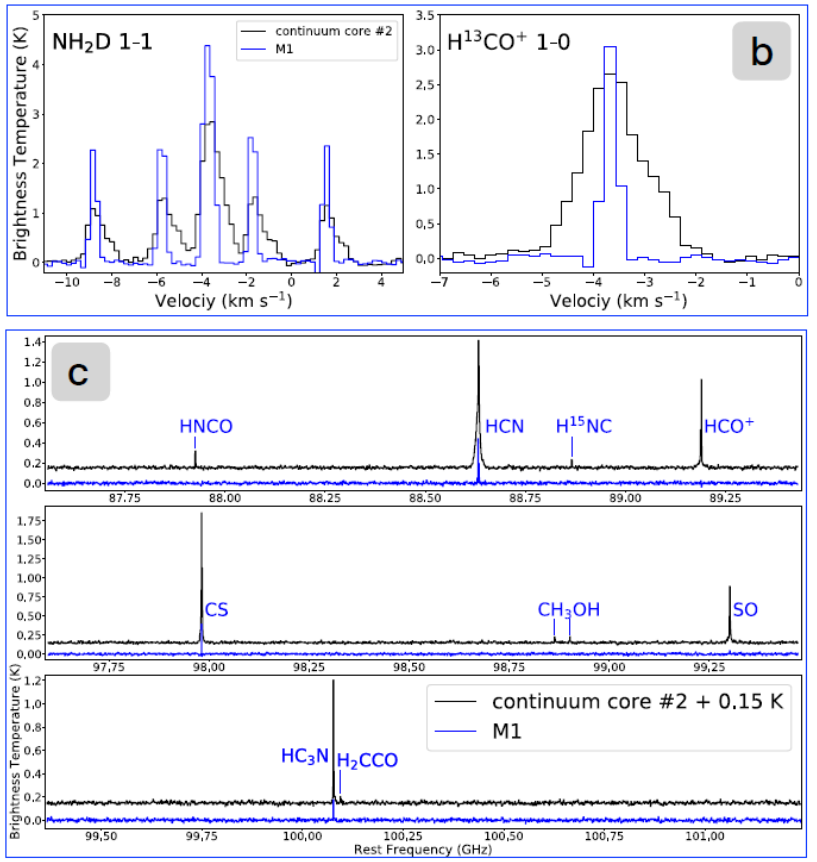

黒線は
Protostellar core
Cont #2

- NH2Dコアは、Cont #2よりも化学的に複雑でない
- Cont #2もいわゆるhot core/corinoではないが。
- NH2Dコアの進化段階は、Cont #2よりも前

NH2Dは星形成活動が見られずに冷たく静穏的

- 全てのNH2Dコアにおいて、星形成の兆候(アウトフロー by HCO+, CS, HCN, SO, HNCOとH2O maser)を調べたが見つからない。
- NH2Dは赤外線の連続波で暗い
- Internal luminosityの上限は~ 1.26 $L_{\odot}$

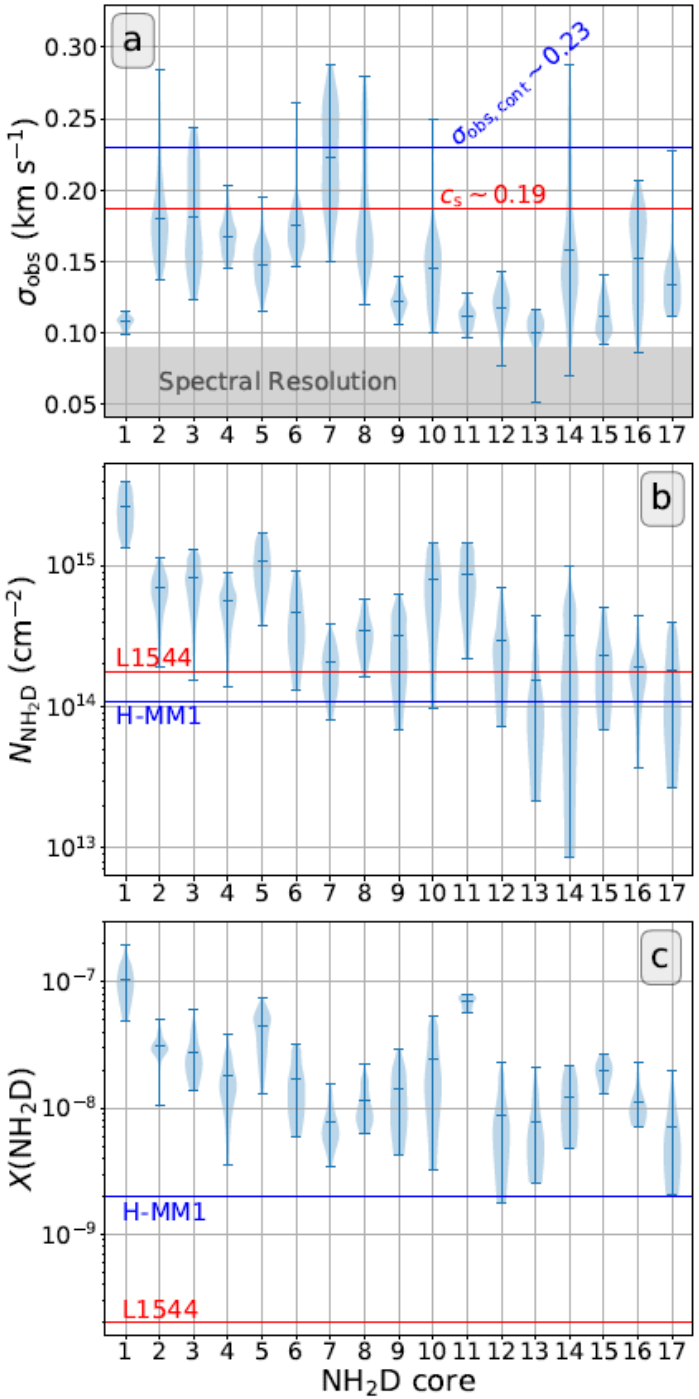

- NH2Dコアでは、熱運動が卓越
- infallの兆候は見えない。
  光学的に厚い輝線の速度分解能がよくないからかも (3.0-3.3 km/s)

- $N_{\mathrm{NH_2D}}$と$X(\mathrm{NH_2D})$(X(NH2D) = N(NH2D)/N(H2))が、
  近傍の星形成領域のprestellar core(H-MM1, L1544)よりも大きい
- JVLAでのNH3の観測から、重元素比を求めると、
  M4で0.25, M10で0.11だった。→ これは他の小質量星形成領域と似てる。
  重水素濃縮がおこる低温環境であるとともに長時間NH3が存在していることを示している。
  - L1544: 0.5+-2 (Crapsi+2007), H-MM1: 0.45+-0.09 (Harju+2017)

- 左の図とは関係ないが
  - 連続波から見積もった質量(Tdust=10Kと仮定)は
    0.13-0.87 Msun → 小質量星形成領域
  - 17個のNH2Dのうち9個が重力的に束縛されている。

H-MM1: Ophuchus
L1544: pre-stellar core

- NH2Dコアは、静穏(速度分散~熱運動)で、NH2D組成比が高く、高いNH3重元素比をもち、3.6-70umで暗い。
- 大質量星団形成雲でのlow mass starless, pre-stellar coreの初検出
- コアには、大きな多様性がある
  - mass: 0.13-14.03 Msun (小質量コアから大質量コアまで同時に形成)
  - age: pre-stellar-Class II (定常的な星形成)
- 大質量コアは中心にあり、小質量コアは広く散らばっている
- NH2Dコアの大部分は、H13CO+で検出された広がったフィラメント構造に関連している。詳細な解析はこれから。

23. A Multi-wavelength Study on the Formation of AFGL 333-Ridge

XiaoLian Liang, Jin-Long Xu, Ye Xu, Jun-Jie Wang ★ We presented a multi-wavelength study of AFGL 333-Ridge. The molecular line data reveals that the AFGL 333-Ridge has two independent velocity components at -50.5 km/s and -48.0 km/s. In the Position-Velocity diagram, the bridge feature connects with two parts that are spatially correlated but separated in velocity. These observational evidences support the scenario that the two velocity components have collided and merged into one molecular cloud. The majority of Class I YSOs are distributed within the collision region, suggesting that the cloud-cloud collision has induced the YSOs formation in the ridge. Using the radio recombination line (RRL) data obtained by the Five-hundred-meter Aperture Spherical radio Telescope (FAST), the RRL velocities of three HII regions are consistent with that of the AFGL 333-Ridge. By comparing the three HII regions' dynamical ages with the collision timescale of the two components, we conclude that the influence of the three HII regions may not drive the two clouds to merge. The formation of the AFGL 333-Ridge is probably due to the expansion of the giant HII region W4.

- 巨大分子雲W4の、AFGL 333-Ridge領域で、二つの速度成分 (-50.5km/sと-48.0 km/s)が見つかった。
- 二つの速度成分は空間的に相補的に分布していて、PV図に二つの速度成分をつなげるbridge構造がある。
  → cloud-cloud collision ?

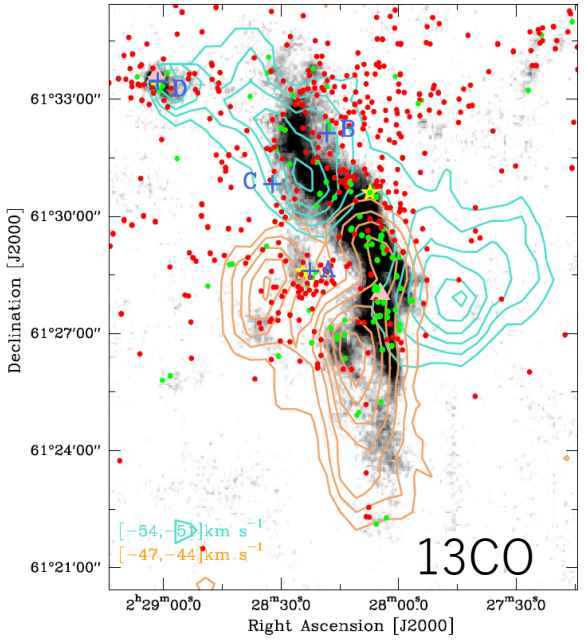

Ridgeに沿ったPV図

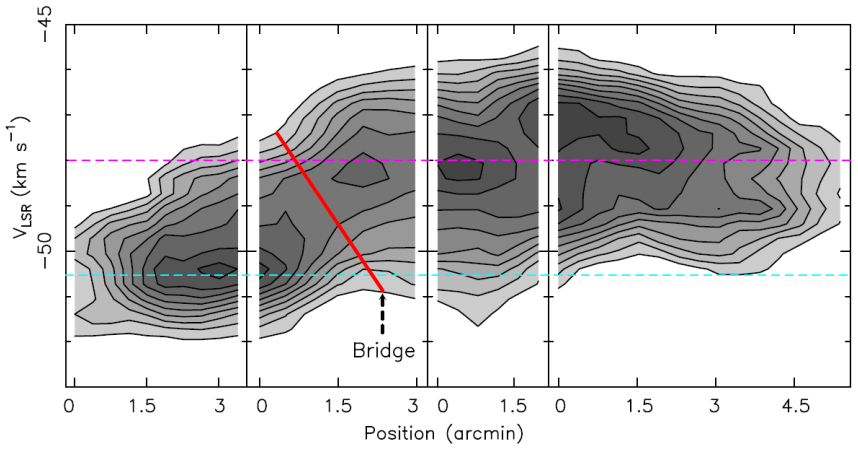

Viewing angleが分からないが、衝突速度に沿った方法から見ていなければ、
速度差は数km/sで、この天体の質量(～10^4Msun)と大きさを考えると、普通に重力収縮とかでも説明できる気もする。

24. **Revealing Ionization Conditions of Sz 102 with Spatially Resolved [Ne III] Microjets**

Chun-Fan Liu, Hsien Shang, Gregory J. Herczeg, Frederick M. Walter ★ Forbidden neon emission lines from small-scale microjets can probe high-energy processes in low-mass young stellar systems. We obtained spatially resolved [Ne III] spectra of the microjets from the classical T Tauri Star Sz 102 using the Hubble Space Telescope Imaging Spectrograph (HST/STIS) at a spatial resolution of 0".1. The blueshifted and redshifted [Ne III] emission both peak in intensity within 0".1 of the star and gradually decay along the flow outward to 0".24. The spatial distribution and extent of the [Ne III] microjet is consistent with a jet that is ionized close to the base and subsequently recombines on a longer timescale than the flow time. Ca II H and K lines are also detected from the redshifted microjet with a line full-width at half-maximum of 170 km/s, consistent with those of other forbidden emission lines, atop a 300-km/s wide stellar component. The launching radius of the Sz 102 jet, inferred from the observed line centroids and the range of inclination angles and stellar masses from the literature, is on the order of 0.03 au. The possible proximity of the launching region to the star allows immediate ionization without distance dilution from the circumstellar ionization sources, most likely keV X-ray flares generated by magnetic reconnection events in the star-disk system, to sustain the observed [Ne III] flux.

- 古典的T Tauri星 Sz102をHST/STISで観測し、micro-jetからのNeIIIを検出。
  - Micro-jetとは、星近くの1秒角スケールで分解されたlaunching regionでのjet構造
- NeIII microjetの空間構造と量から、根本(～0.03 au)で電離され、
  伝播時間スケールより長い時間で再結合していることが示唆。
- 衝突電離されている動力学的な証拠はなかった
  → 星のそばでの、keV X-rayを出すフレアが電離に効いているかもしれない。
  活動的な原始星の中には、磁気ループが星半径の数倍くらいないと説明できない巨大フレアが起こっている。

25. Do ultra compact dwarf galaxies form monolithically or as merged star cluster complexes?

Hamidreza Mahani, Akram Hasani Zonoozi, Hosein Haghi, Tereza Jerabkova, Pavel Kroupa, Steffen Mieske

★ Some ultra-compact dwarf galaxies (UCDs) have elevated observed dynamical V-band mass-to-light ($M/L_{\rm V}$) ratios with respect to what is expected from their stellar populations assuming a canonical initial mass function (IMF). Observations have also revealed the presence of a compact dark object in the centers of several UCDs, having a mass of a few to 15% of the present-day stellar mass of the UCD. This central mass concentration has typically been interpreted as a super-massive black hole, but can in principle also be a sub-cluster of stellar remnants. We explore the following two formation scenarios of UCDs, i) monolithic collapse and ii) mergers of star clusters in cluster complexes as are observed in massively star-bursting regions. We explore the physical properties of the UCDs at different evolutionary stages assuming different initial stellar masses of the UCDs and the IMF being either universal or changing systematically with metallicity and density according to the Integrated Galactic IMF (IGIMF) theory. While the observed elevated $M/L_{\rm V}$ ratios of the UCDs cannot be reproduced if the IMF is invariant and universal, the empirically derived IMF which varies systematically with density and metallicity shows agreement with the observations. Incorporating the UCD-mass-dependent retention fraction of dark remnants improves this agreement. In addition we apply the results of N-body simulations to young UCDs and show that the same initial conditions describing the observed $M/L_{\rm V}$ ratios reproduce the observed relation between the half-mass radii and the present-day masses of the UCDs. The findings thus suggest that the majority of UCDs that have elevated $M/L_{\rm V}$ ratios could have formed monolithically with significant remnant-mass components that are centrally concentrated, while those with small M/L_V values may be merged star-cluster complexes.

26. **PENELLOPE: the ESO data legacy program to complement the Hubble UV Legacy Library of Young Stars (ULLYSES) I. Survey presentation and accretion properties of Orion OB1 and σ-Orionis**

PENELLOPE team - C. F. Manara et al.

★ The evolution of young stars and disks is driven by the interplay of several processes, notably accretion and ejection of material. Critical to correctly describe the conditions of planet formation, these processes are best probed spectroscopically. About five-hundred orbits of the Hubble Space Telescope (HST) are being devoted in 2020-2022 to the ULLYSES public survey of about 70 low-mass (M<2Msun) young (age<10 Myr) stars at UV wavelengths. Here we present the PENELLOPE Large Program that is being carried out at the ESO Very Large Telescope (VLT) to acquire, contemporaneous to HST, optical ESPRESSO/UVES high-resolution spectra to investigate the kinematics of the emitting gas, and UV-to-NIR X-Shooter medium-resolution flux-calibrated spectra to provide the fundamental parameters that HST data alone cannot provide, such as extinction and stellar properties. The data obtained by PENELLOPE have no proprietary time, and the fully reduced spectra are made available to the whole community. Here, we describe the data and the first scientific analysis of the accretion properties for the sample of thirteen targets located in the Orion OB1 association and in the sigma-Orionis cluster, observed in Nov-Dec 2020. We find that the accretion rates are in line with those observed previously in similarly young star-forming regions, with a variability on a timescale of days of <3. The comparison of the fits to the continuum excess emission obtained with a slab model on the X-Shooter spectra and the HST/STIS spectra shows a shortcoming in the X-Shooter estimates of <10uncertainty. Its origin can be either a wrong UV extinction curve or due to the simplicity of this modelling, and will be investigated in the course of the PENELLOPE program. The combined ULLYSES and PENELLOPE data will be key for a better understanding of the accretion/ejection mechanisms in young stars.

- ULLYSES program by HST
  - 約70個の若い(<10Myr)小質量(<2Msun)をUVで観測(2020-2022)。質量降着や放出を探る。
- PENELLOPE (進行中)
  - 上記の天体をESO VLTで、可視光と赤外で観測 → 中心星の特徴、星間減光、円盤風、ジェット、など